Cell Reports
Report
ACCESS
CellPress

The Intracellular Na^+/H^+ Exchanger NHE7 Effects a Na^+-Coupled, but Not K^+-Coupled Proton-Loading Mechanism in Endocytosis

Nina Milosavljevic,[1,4] Michaël Monet,[1] Isabelle Léna,[1] Frédéric Brau,[2] Sandra Lacas-Gervais,[3] Sylvain Feliciangeli,[2] Laurent Counillon,[1,5,*] and Mallorie Poët[1,5]
[1]Université Nice-Sophia Antipolis, LP2M CNRS-UMR 7370, Faculté de Médecine, 28 Avenue de Valombrose, 06107 Nice, France
[2]Université Nice-Sophia Antipolis, IPMC CNRS-UMR 7275, 660 Route des Lucioles Sophia Antipolis, 06560 Valbonne, France
[3]Université Nice-Sophia Antipolis, CCMA Faculté des Sciences Parc Valrose, 06108 Nice, France
[4]Present address: Faculty of Life Sciences, University of Manchester, Oxford Road, AV Hill Building, Manchester M13 9PT, UK
[5]Co-senior author
*Correspondence: laurent.counillon@unice.fr
http://dx.doi.org/10.1016/j.celrep.2014.03.054

SUMMARY

Vesicular H^+-ATPases and ClC-chloride transporters are described to acidify intracellular compartments, which also express the highly conserved Na^+/H^+ exchangers NHE6, NHE7, and NHE9. Mutations of these exchangers cause autism-spectrum disorders and neurodegeneration. NHE6, NHE7, and NHE9 are hypothesized to exchange cytosolic K^+ for H^+ and alkalinize vesicles, but this notion has remained untested in K^+ because their intracellular localization prevents functional measurements. Using proton-killing techniques, we selected a cell line that expresses wild-type NHE7 at the plasma membrane, enabling measurement of the exchanger's transport parameters. We found that NHE7 transports Li^+ and Na^+, but not K^+, is nonreversible in physiological conditions and is constitutively activated by cytosolic H^+. Therefore, NHE7 acts as a proton-loading transporter rather than a proton leak. NHE7 mediates an acidification of intracellular vesicles that is additive to that of V-ATPases and that accelerates endocytosis. This study reveals an unexpected function for vesicular Na^+/H^+ exchangers and provides clues for understanding NHE-linked neurological disorders.

INTRODUCTION

Eukaryotic single-membrane organelles possess a finely tuned acidic luminal pH, which is crucial for the compartmentalization of cellular events and for the maturation, trafficking, recycling, and degradation of proteins (Mellman, 1992). This acidification has been widely reported to be produced by vacuolar H^+-ATPases (Marshansky and Futai, 2008), coupled to vesicular ClC chloride transporters (Jentsch, 2007) that neutralize the charge gradient produced by proton pumping. Defects in genes encoding these transporters produce spectacular phenotypes in knockout mice or human patients (Kornak et al., 2000; Günther et al., 2003; Kasper et al., 2005; Poët et al., 2006).

Highly conserved Na^+/H^+ exchangers, NHE6, 7, and 9, are also expressed in intracellular compartments (Numata and Orlowski, 2001; Nakamura et al., 2005). NHE6 mutations have been identified in families with Angelman and Christianson syndromes (Gilfillan et al., 2008; Mignot et al., 2013), whereas NHE9 has been linked with family-based autism (Morrow et al., 2008) and attention deficit hyperactivity disorder (Lasky-Su et al., 2008; Franke et al., 2009). NHE7 has recently been identified as a novel target gene for Alzheimer's disease (Meda et al., 2012) and X-linked mental retardation contiguous genes syndromes (Zhang et al., 2006). It has been proposed that NHE7 works in a reverse mode compared to plasma membrane NHEs, by using cytosolic potassium in exchange to vesicular protons. This might account, at least partly, for the vesicular proton leak (Demaurex et al., 1998; Llopis et al., 1998) that might contribute to set their steady-state pH. However, such a proposed important biological function has to be supported by data specifying the affinities for transported cations, the sense of transport, and its regulation. This has been so far prevented by the intracellular localization of these NHEs.

Here, we used proton-killing techniques to select a fibroblast cell line that expresses the wild-type NHE7 at the plasma membrane and used it to measure the above-mentioned parameters. We show that contrary to the prevailing model, NHE7 rather functions as a proton-loading transporter in a manner additive to V-ATPases. This function is in excellent accordance with the neuronal distribution of the NHE7 protein also displayed in this study.

RESULTS

Selection of the PM-NHE7 Cell Line

We used plasma membrane NHE-deficient PS120 fibroblasts (Pouysségur et al., 1984), which also do not express NHE6, 7, 8, and 9, as shown by quantitative PCR (qPCR) and western blotting (Figure S1). They were stably transfected with the human NHE7 (*SLC9A7*) cDNA to yield the WT-NHE7 cell line.

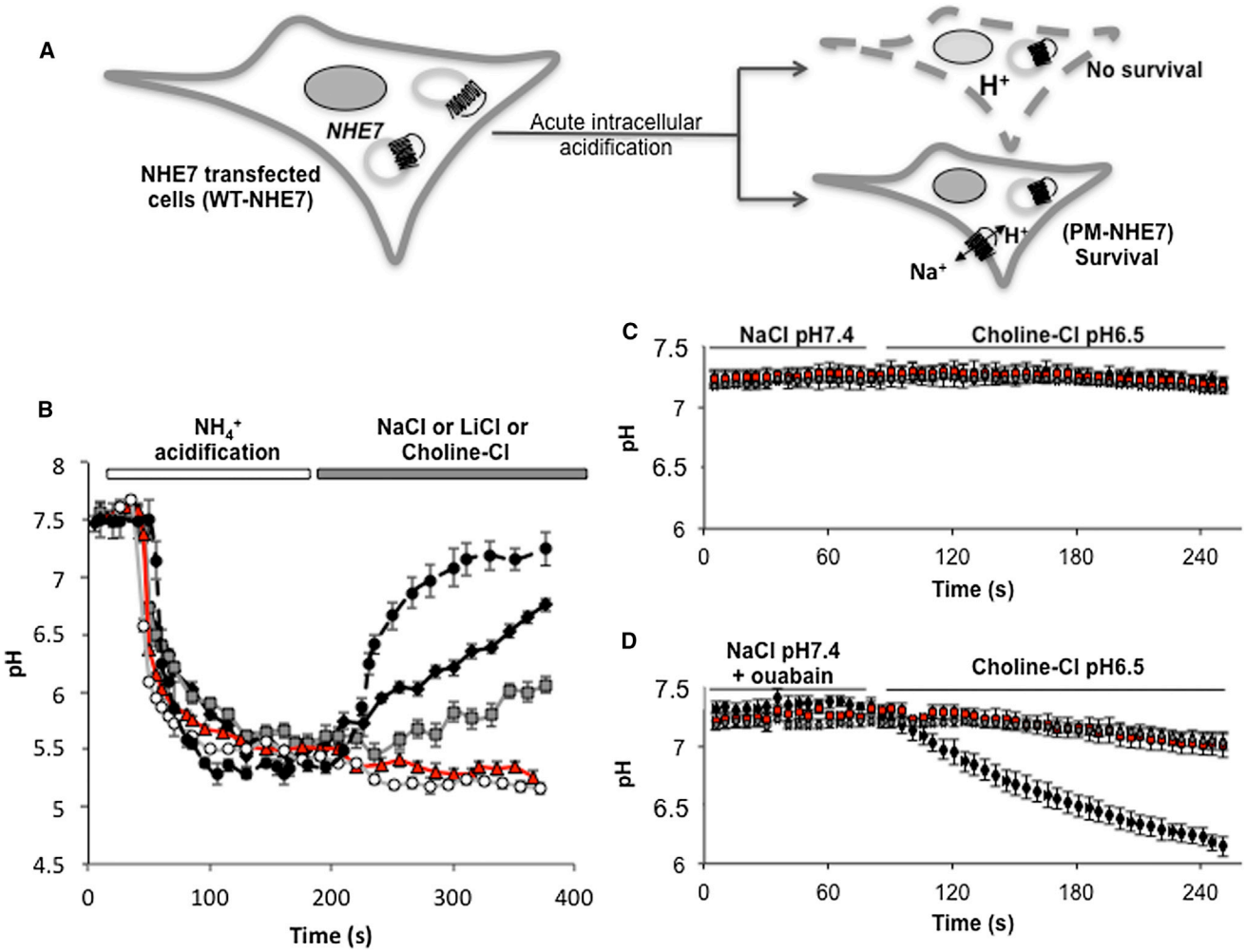

Figure 1. NHE7 Expression at the Plasma Membrane of PMNHE7 Cells

(A) Selection of cells expressing a functional nonmutated and nontagged NHE7 at the plasma membrane.

(B) Intracellular pH variations following an intracellular acidification: PM-NHE7 cells with 140 mM extracellular NaCl, dark diamonds; 140 mM LiCl, gray squares; 140 mM choline chloride, circles; and WT-NHE7 cells with 140 mM extracellular NaCl, red triangles. NHE1-transfected PS120 cells with 140 mM NaCl are shown as dots.

(C) Reverse mode: intracellular pH variations in the presence of extracellular 140 mM choline chloride at pH 6.5 for PM-NHE7 cells, red squares; pHygro-PS120 cells, gray diamonds; and NHE1-transfected PS120 cells, dots.

(D) Reverse mode after Na^+ loading (39.09 ± 0.03 mM intracellular Na^+): PM-NHE7, squares; pHygro-PS120, gray diamonds; and NHE1-transfected PS120 cells, dots.

Error bars represent SEM.

WT-NHE7 cells were then submitted to repeated acute acid loads (Supplemental Experimental Procedures), so that only variants able to extrude protons by expressing a functional NHE7 at their plasma membrane will be positively selected (Figure 1A). This led to the isolation of the Plasma Membrane-NHE7 (PM-NHE7) cell line that, in contrast to the parental WT-NHE7 cells (Figure 1B), could use extracellular sodium or lithium to recover from acute intracellular acidifications. NHE7 plasma membrane expression was verified (1) by cell-surface biotinylation assays and (2) by showing that two distinct NHE7 siRNAs decreased its membrane expression together with exchange activity (Figure S2). The NHE7 cDNA from PM-NHE7 cells was also entirely resequenced to verify that no mutations were present. Transmission electron microscopy showed undamaged ER, Golgi, mitochondria, and a similar intracellular organization to that of WT-NHE7 cells (Figures S3A–S3D). Importantly, when the TWIK1 vesicular K^+ channel (Feliciangeli et al., 2010) was transfected in our cell lines, cell-surface biotinylation assays revealed a strong enrichment at the plasma membrane of PM-NHE7 cells, compared to WT-NHE7 and control pHygro-PS120 cells (Figures S3E and S3F). Expressing vesicular membrane proteins at the plasma membrane is therefore not a specific deficiency toward NHE7 but instead a more general feature of PM-NHE7 cells. These cells

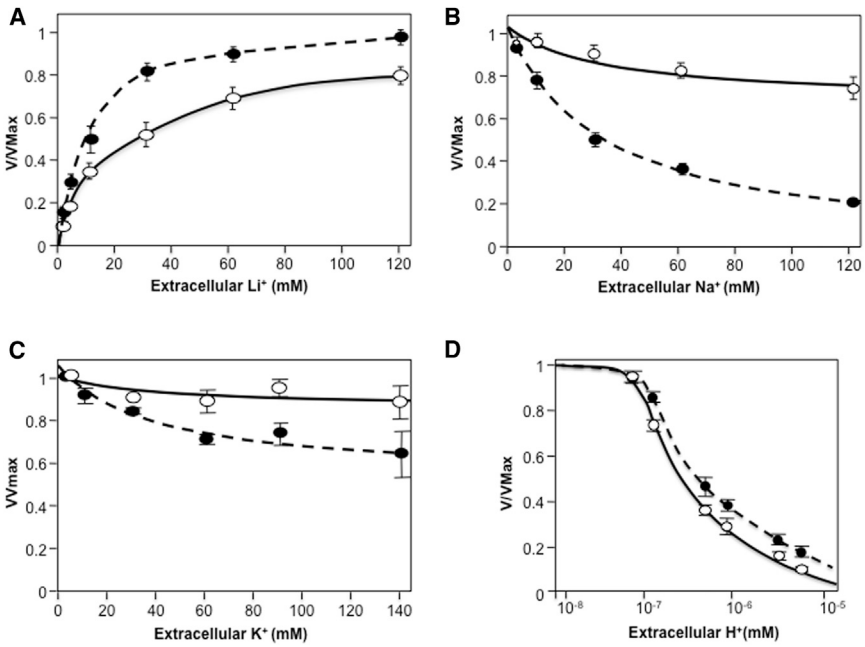

Figure 2. Dose-Response Curves for NHE7 and NHE1

Cells were acidified as in Figure 1B, and initial rates of Lithium uptake were measured using 1 min kinetics. NHE7: lines, circles; NHE1: dotted lines, dots.

(A) Dose-response curve for extracellular lithium.

(B) Competition of different concentrations of extracellular sodium on 1 mM extracellular lithium uptake.

(C) Competition of extracellular potassium on 1 mM extracellular lithium uptake.

(D) Competition of extracellular proton on 1 mM extracellular lithium uptake.

Error bars represent SEM.

could be valuable tools to study vesicular proteins by expressing them at the plasma membrane.

Ion Transport Reversibility and Selectivity

The external medium facing NHE7 in PM-NHE7 cells corresponds to the vesicular lumen in WT-NHE7 cells (Figure 1A). The incubation of PM-NHE7 cells in a sodium- and potassium-free acidic external medium (pH 6.5) did not significantly change the intracellular pH (Figure 1C). Accordingly, NHE7 cannot exchange cytosolic K^+ with extracellular or vesicular protons.

Likewise, we could not detect reversibility using the same extracellular medium when the cytosol was preloaded with Na^+ (1 mM ouabain preincubation in K^+-free medium, Figure 1D) or with Li^+ (Figure S3G). Thus, reversibility, as shown for NHE1 in the tested conditions, is not a general feature of the NHE family.

The affinity constants for extracellular Na^+, Li^+, and K^+ ions were determined for NHE7 and compared to those of the plasma membrane NHE1. Lithium was used for measuring initial uptake rates (Figure S2G), because it is transported by NHE7 and can be quantified with very high sensitivity by atomic absorption spectroscopy (Milosavljevic et al., 2010). The Km for extracellular Li^+ was 16.3 ± 1.8 mM (Figure 2A), similar to that of NHE1 (9 ± 1.4 mM). Competition of different extracellular Na^+ concentrations with lithium transport (1 mM, Figure 2B), yielded an estimated Km value of 240 ± 26 mM for NHE7, compared to 31 ± 4.7 mM for NHE1. Sequence alignments, which may explain this large difference, are shown and discussed in Figure S4A and Supplemental Discussion.

Extracellular K^+ did not decrease NHE7 lithium transport (Figure 2C), indicating that K^+ cannot bind the NHE7 extracellular/vesicular transport site. Taken together with the results of Figure 1C, potassium is not a substrate of NHE7.

NHE7 Inhibition by Acylguanidines and Vesicular Protons

When tested on NHE7, amiloride, 5-(N-ethyl-N-isopropyl)-amiloride (EIPA) and cariporide yielded similar Ki values as those obtained for the plasma membrane NHE1 (Figure S3H). NHE7 is subsequently not "amiloride resistant" as previously reported (Numata and Orlowski, 2001). NHE7 was also blocked by extracellular/luminal protons, with a similar inhibition constant as for NHE1 ($2 \times 10^{-7} \pm 7 \times 10^{-8}$ M and $4.3 \times 10^{-7} \pm 1.6 \times 10^{-7}$ M, respectively; Figure 2D).

Given that these inhibitors and vesicular protons compete for sodium binding, their effects will be enhanced in vivo because of NHE7 low affinity for sodium. This may provide clues for the side effects of previously believed NHE1-specific inhibitors.

Cytoplasmic Protons

Regulation by cytosolic protons is an essential feature of Na^+/H^+ exchangers. We found a very unusual response for NHE7, which is Michaelian, with a high affinity for protons (Km = 2.5 10^{-7} ± 3.53 10^{-9}M) compared to NHE1 (Figure 3A) that is cooperatively regulated (Lacroix et al., 2004). In contrast to previous hypotheses, NHE7 can only use the high sodium concentration initially available in endocytic vesicles (Scott and Gruenberg, 2011) to constitutively import cytoplasmic protons to their lumen (Figure 3B).

NHE7 Acidifies Early Endosomes

In WT-NHE7 cells, NHE7 colocalized with the transferrin receptor (Pearson coefficient = 0.68 ± 0.01, n = 7, Figure 3C), and with TGN38 (Pearson coefficient = 0.66 ± 0.08, n = 5, Figure 3D) in accordance with studies showing NHE7 in the receptor-mediated endocytosis pathway (Lin et al., 2005) and in TGN (Numata and Orlowski 2001) (see also Figure S1C). A similar colocalization with the transferrin receptor was found in rat hippocampus pyramidal neurons (Pearson coefficient = 0.616 ± 0.04, n = 5, Figure 3E), whereas a very different pattern was observed for TGN38 (Pearson coefficient = 0.11 ± 0.05 n = 4, Figure 3F). In neurons, this points toward a predominant role of NHE7 in the endocytic pathway.

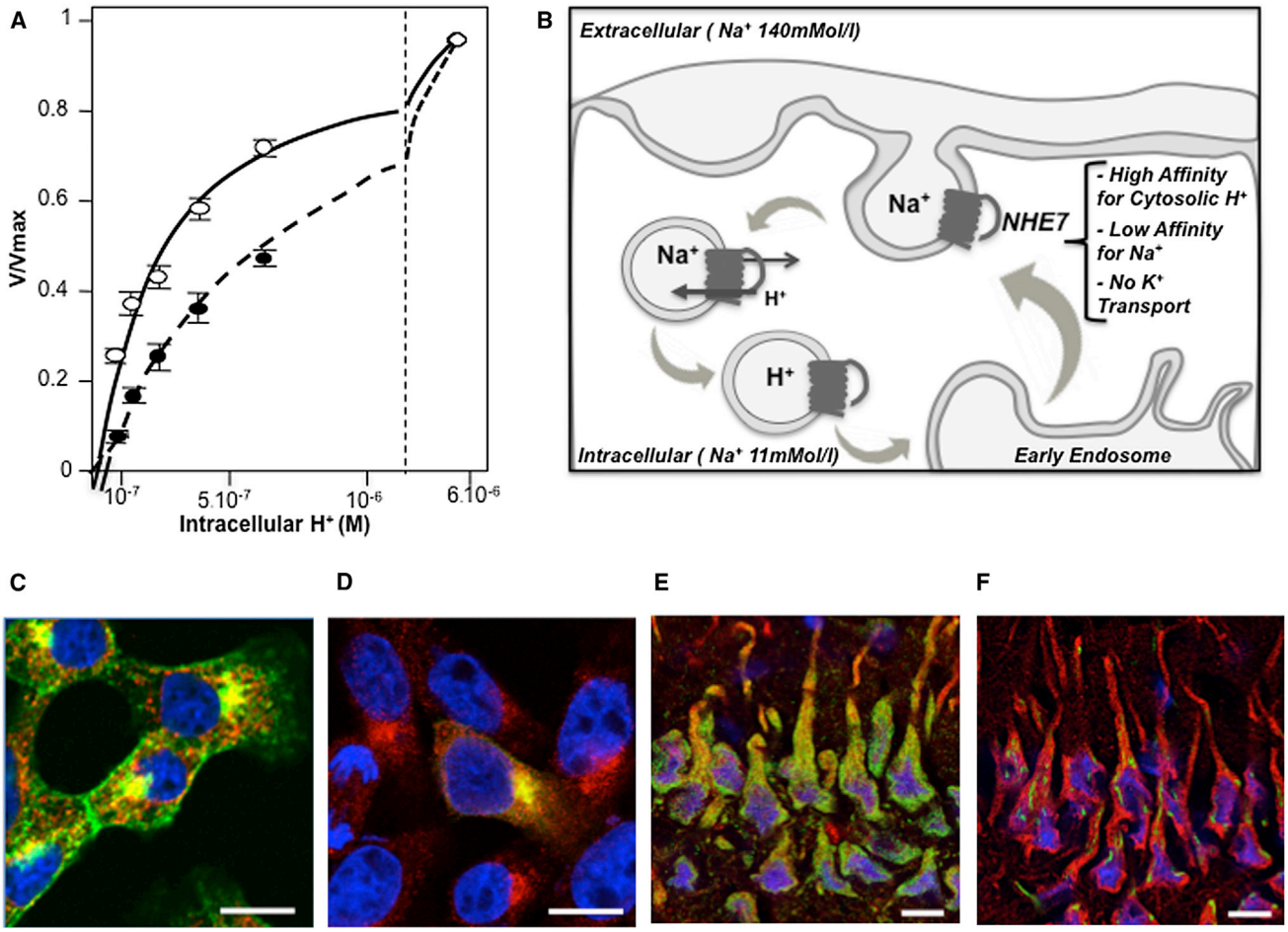

Figure 3. NHE7 Interaction with Intracellular Protons, Mechanism of Action, and Subcellular Localization

(A) Dose response of NHE7 (lines, circles) and NHE1 (dotted lines, dots) activities for intracellular proton. Intracellular pH was clamped at different values using nigericin acidification (Lacroix et al., 2004). Initial rates of lithium uptake were then measured.

(B) Model deduced from NHE7 measured affinities for its transported cations and their physiological concentrations.

(C–F) Colocalization of NHE7 (red), transferrin receptor, or TGN38 (green). Blue: HOE33258. Scale bar, represents 10 μm. (C) NHE7 and transferrin receptor in WT-NHE7 fibroblasts. (D) NHE7 and TGN38 in WT-NHE7 fibroblasts. (E) NHE7 and transferrin receptor in rat brain hippocampus pyramidal cells. (F) NHE7 and TGN38 in rat brain hippocampus pyramidal cells.

Error bars represent SEM.

The pH of transferrin-positive endocytic vesicles and endosomes was measured in live cells using pH-sensitive Fluorescein coupled to transferrin (Teter et al., 1998). In both pHygro-PS120 and WT-NHE7 cells, these compartments displayed similar steady-state pH (6.42 ± 0.03 and 6.47 ± 0.10, respectively, Figures 4A and 4B). However, in the presence of 10 μM EIPA, WT-NHE7 cells displayed a significantly increased intravesicular pH (6.91 ± 0.06, ANOVA test $p < 0.01$). Conversely, the V-ATPase inhibitor bafilomycin produced an alkalinization to pH 7.11 ± 0.08, which reached 7.40 ± 0.07 in the presence of 10 μM EIPA ($p < 0.05$). In the pHygro-PS120 cells, EIPA did not produce significant effects on vesicular pH (6.61 ± 0.04), whereas bafilomycin alone was able to alkalinize endosomes to 7.41 ± 0.05 (Figure 4B), with no significant additive effect of EIPA. Similar results were obtained using sodium-free extracellular medium instead of adding EIPA (Figures S4B and S4C). Taken together, these important pH differences are in excellent agreement with an acidifying role of NHE7 (Figure 3B).

NHE7 Enhances the Rate of Endocytosis

A comparable steady-state endosomal pH in the presence or in the absence of NHE7 suggests a role of this exchanger in the early phases of endocytosis. To investigate this point, pH-insensitive Alexa 555 transferrin was bound at 4°C in WT-NHE7 or in pHygro-PS120 cells. Rates of fluorescence transfer into early endosomal perinuclear clusters after shifting temperature to 37°C were followed using time-lapse spinning disk confocal microscopy. As shown in Figure 4C (see also Figure S4D; Movies S1 and S2), the rate of transferrin import is 3.3-fold faster

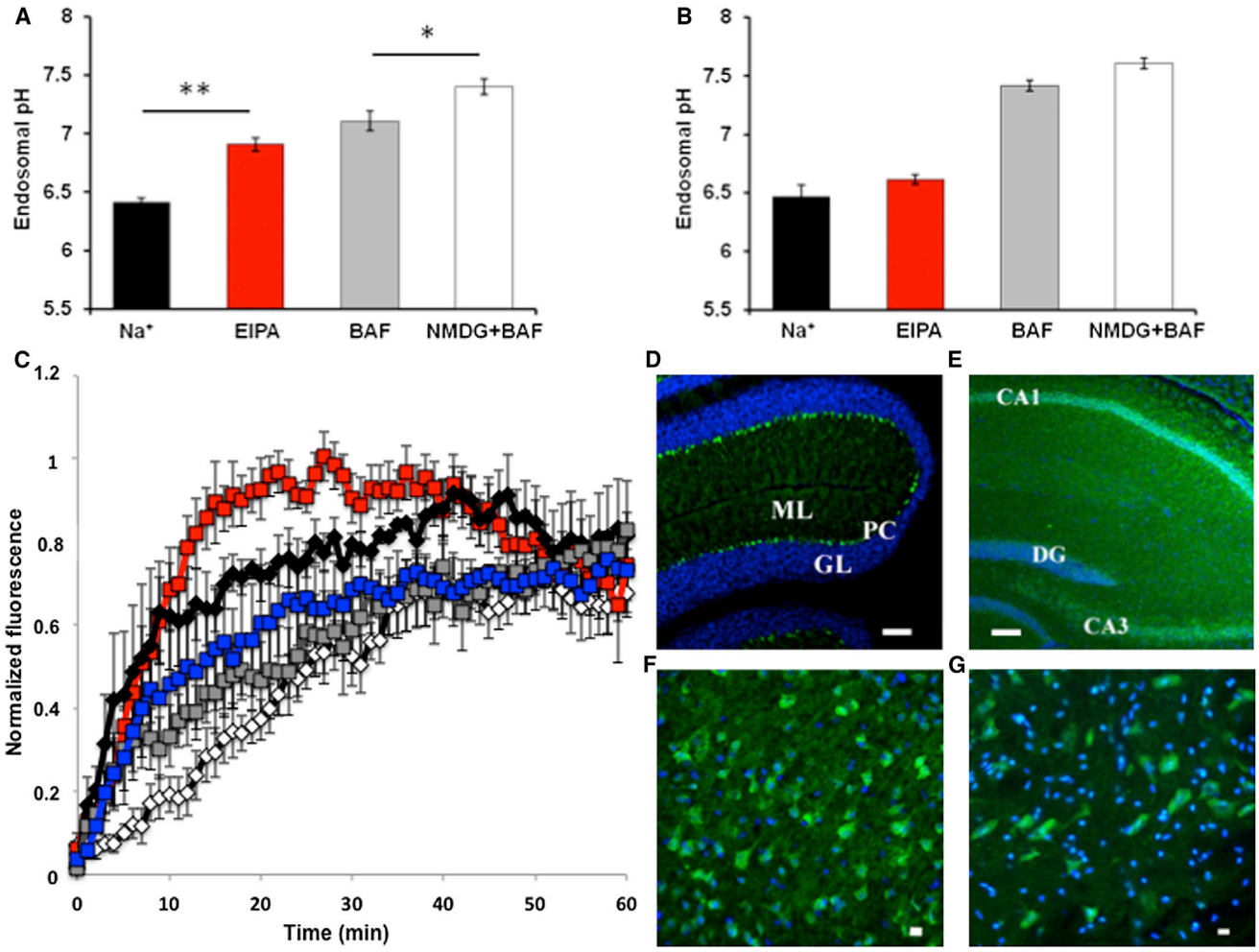

Figure 4. NHE7 Role in Endocytosis and Localization in Brain Sections

(A) Steady-state endosomal pH measurements in WT-NHE7 cells using fluorescein coupled to transferrin in control conditions or with the NHE inhibitor EIPA (10 μM) and/or the V-ATPase inhibitor bafilomycin (BAF, 500 nM). ANOVA test: *$p < 0.05$; **$p < 0.01$.

(B) Steady-state endosomal pH measurements in the pHygro-PS120 control cells in the same conditions as in Figure 4A.

(C) Quantification of Alexa 555 transferrin uptake measured by spinning disk confocal microscopy in the pHygro-PS120 control cells and in the WT-NHE7 cells. Endocytosis was quantified as the kinetics of normalized fluorescence internalization in intracellular clusters. WT-NHE7, squares (red, pHe = 7.4; gray, pHe = 8; blue, 30 mM external NaCl at pHe = 7.4 in isotonic conditions); pHygro-PS120, diamonds (white, pHe = 7.4; dark, pHe = 7).

(D–G) NHE7 localization in mouse brain sections. Immunohistochemistry was performed as described in Experimental Procedures using the mouse NHE7 antibody (green) and HOECHST33258 for nuclear staining. (D) Cerebellum; PC, Purkinje cells; GL, granular layer; ML, molecular layer. Scale bar represents 100 μm. (E) Hippocampus: CAI and CAIII: pyramidal cells of CAI and CAIII. DG, dentate gyrus. Scale bar represents 100 μm. (F) Cortex (layers II–V), scale bar represents 10 μm. (G) Brainstem (motor nucleus VII). Scale bar represents 10 μm.

Error bars represent SEM.

in WT-NHE7 cells than in control cells. This effect of NHE7 was decreased by a lower extracellular sodium concentration (30 mM NaCl in isotonic medium, Figure 4C) or by 10 μM EIPA (Movie S3).

To determine whether this enhanced rate was indeed caused by NHE7-mediated proton loading, we reasoned that, for NHE-deficient cells, this could be mimicked by a slightly acidic extracellular pH that would lower the pH of endocytic vesicles. Indeed, transferrin uptake in pHygro-PS120 cells was accelerated at an external pH 7.0 (Figure 4C; Movie S4). Conversely, increasing extracellular pH to 8.0 slowed down endocytosis in WT-NHE7 cells (Figure 4C).

NHE7 Is Localized in Large Integrative Neurons

To further understand NHE7-related cerebral deficiencies, we conducted an extensive screen for an antibody that could detect specifically NHE7 (see Figures S1 and S2). In brain sections (Experimental Procedures), we observed a very typical expression pattern in large neurons of the central nervous system such as Purkinje cells in the cerebellum, pyramidal cells in

hippocampus and cortex, or motor neurons in brainstem (Figures 4D–4G).

DISCUSSION

The first major finding of this work is that NHE7 does not work as a K^+-coupled proton leak but instead is an acidifier of intracellular compartments. Actually, this is not surprising, because the large sodium gradient between endocytic vesicles and the cytosol will allow such an exchanger to produce significant acidifications. Indeed, NHE7 and V-ATPase inhibitors both produced a similar increase in vesicular pH (Figure 4A). NHE7 is not able to transport potassium, is inhibited by vesicular protons, and has low affinity for sodium. Given the cytosolic ionic composition, such an amazingly redundant set of safety mechanisms prevents any possible shift to a reverse mode that would dissipate the vesicular pH gradient.

The second major finding is that NHE7 proton loading enhances the rate of endocytic trafficking. Interestingly, this can be mimicked by a moderate acidification of extracellular medium (Figure 4C), a situation that could be found in ischemic or inflammatory situations. Such an effect has also been reported for antigen processing by dendritic cells (Vermeulen et al., 2004). The molecular mechanisms by which luminal pH is sensed by cytosolic effectors of donor and acceptor compartments are thus far not fully understood and might involve pH-dependent coat assembly (Clague et al., 1994; Aniento et al., 1996; Gu and Gruenberg, 2000). Additionally, Arf6 and ARNO bind endosomal membranes in a pH-dependent manner (Maranda et al., 2001) and also interact with the V-ATPase a2 and c subunits (Hurtado-Lorenzo et al., 2006).

The cognitive and neurodegenerative defects of the human intracellular NHE mutants (Gilfillan et al., 2008; Morrow et al., 2008; Zhang et al., 2006; Garbern et al., 2010) or mice models (Strømme et al., 2011) were reminiscent of those observed for the defects of (1) ClC transporters involved in vesicular acidification (Poët et al., 2006; Kasper et al., 2005), or (2) of vesicular Cathepsins working at acidic pH (Felbor et al., 2002). These phenotypes were difficult to reconcile with the previous model of alkalinizing vesicular NHEs but are in excellent accordance with the acidifying role of NHE7. Furthermore, we show that the NHE7 protein displays a spectacular expression in large neurons that constantly integrate inputs from numerous afferents (Figures 4D–4G). The enhanced vesicular trafficking provided by NHE7 is expected to accelerate protein turnover and enhance plasticity in such neurons. Taken together, these elements strongly point toward a specific connection between NHE7 localization, acidifying role and integrative brain functions. It may also provide clues for the recent association between NHE7 and late-onset Alzheimer's disease (Meda et al., 2012).

Lithium yielded slower rates of pH recovery than sodium in PM-NHE7 cells (see Figure 1B). In vivo, this cation is expected to slightly inhibit NHE7, in accordance with standard Michaelis-Menten kinetics demonstrating that a low Km associated with a reduced rate is the hallmark of a limiting recycling step into active state after ion translocation. Interestingly, lithium concentrations that can be reached in cerebral fluid of patients treated for bipolar disorders (Lee et al., 2012) are in the range of its Km value for NHE7. Therefore, our findings identify NHE7 and possibly the other intracellular NHEs as targets for lithium action.

EXPERIMENTAL PROCEDURES

Selection of PM-NHE7 Cell Line

NHE-deficient fibroblasts (PS120 cell line) were stably transfected with NHE7 cDNA (pIRESHyg3 Vector, Clontech) to generate the WT-NHE7 cell line. A control pHygro-PS120 control cell was generated by transfecting a nonrecombinant pIRESHyg3 vector. WT-NHE7 cells were submitted to repeated acidification using a 50 mM NH_4^+ prepulse followed by 1 hr recovery in 120 mM NaCl, until selection of a cell line (PM-NHE7) stably surviving this acidification. See Supplemental Experimental Procedures.

Intracellular pH Measurements

Cells were loaded with BCECF/AM and excited at 490 and 450 nm. Images were recorded and treated using Axon Imaging Workbench. Calibration was performed using 140 mM K^+ 5 μM nigericin solutions ranging from pH 6.5 to 7.4.

pH Measurements in Transferrin-Positive Compartments

Cells were incubated with 50 mg/ml fluorescein-coupled transferrin (pH 7.4) for 10 min at 37°C in the absence of bicarbonate. After rinse, 490 nm/450 nm fluorescence ratios were recorded for 5 min at room temperature. Calibration was performed using nigericin/monensin as described in Teter et al. (1998).

Measurement of Initial Rates of NHE7

Measurements were performed by fast kinetics of Li^+ uptake as described in Milosavljevic et al. (2010). Li^+ was measured using atomic absorption spectroscopy (Zeeman furnace system, iCE3000 series, Thermo Scientific).

Immunostaining

Immunostainings were performed in fibroblasts after 4% paraformaldehyde (PFA) fixation, BSA, and NGS blocking and saponin permeabilization. Mouse brain sections were prepared as described in Poët et al. (2006). The experimental protocol was approved by the local councils for animal care and was conducted according to the French law for animal care. Antibodies were as follows: primary antibodies were rabbit anti-NHE7 (1:500; MBL) and mouse antitransferrin receptor (1:1,000; Invitrogen). Secondary antibodies were anti-rabbit and/or anti-mouse immunoglobulin G coupled to Alexa Fluor 488 or 594 (Invitrogen).

Confocal Microscopy

We used a Laser Scanning Confocal Microscope (LSM780, Carl Zeiss) equipped with a AxioObserver inverted microscope, using a Plan Apochromat 63×/1.4 NA oil immersion objective (IPMC Imaging core facility, partner of MICA [Microscopy Imaging Côte d'Azur]).

For time-lapse confocal microscopy, 200 μg/ml Alexa 555 transferrin (Invitrogen) was bound for 10 min at 4°C to WT NHE7 or control pHygro-PS120 cells. The cells were rinsed and mounted on a spinning disk confocal microscope UltraviewVox (PerkinElmer) in 2 ml of medium still at 4°C. Temperature was switched to 37°C, and one image was taken every minute for 60 min. Endocytosis was quantified as the normalized fluorescence accumulation in intracellular clusters as a function of time.

Data and Image Treatment and Statistical Analysis

Image treatment and quantitation were performed using NIH ImageJ (Schneider et al., 2012). Data were compiled using Microsoft Excel software and fitted using SigmaPlot or IgorPro software. Curves are compiled from at least five independent experiments, in which experimental points are at least duplicates. Data are presented as mean values and SEM (error bars). Constants are provided with the error of the fits. The treatment groups were compared by one-way ANOVA. Differences were considered significant if $p < 0.05$ (*) and $p < 0.01$ (**).

SUPPLEMENTAL INFORMATION

Supplemental Information includes Supplemental Experimental Procedures, Supplemental Discussion, four figures, and four movies and can be found with this article online at http://dx.doi.org/10.1016/j.celrep.2014.03.054.

AUTHOR CONTRIBUTIONS

N.M. selected the PM-NHE7 cells and determined the kinetics parameters of NHE7 and endosomal pH. M.M. performed the cell-surface biotinylation and siRNA experiments. I.L. determined the cerebral localization of the NHE7 protein. F.B. set up the confocal and spinning disk time-lapse microscopy experiments. S.L.-G. performed the electron-microscopy experiments. S.F. performed cellular localization experiments. L.C. wrote the manuscript. L.C. and M.P. codesigned and cosupervised the work.

ACKNOWLEDGMENTS

This work was supported by the University of Nice-Sophia Antipolis, the ANR (JCJC SVSE1 NHEint), and the CNRS. N.M. was funded by the Basileus EMECW project. We thank Drs. Jacques Barhanin (LP2M CNRS-UMR 7370), Bruno Antonny (IPMC, CNRS-UMR 7275), and Mireille Cormont (C3M INSERM-U 1065) for fruitful discussions, Dr. Ellen Van Obberghen-Schilling (IBV CNRS-UMR 7277) for critical reading of the manuscript, and Fabien Labbal (LP2M CNRS-UMR 7370) for assistance in cell culture.

Received: February 28, 2013
Revised: August 1, 2013
Accepted: March 20, 2014
Published: April 24, 2014

REFERENCES

Aniento, F., Gu, F., Parton, R.G., and Gruenberg, J. (1996). An endosomal beta COP is involved in the pH-dependent formation of transport vesicles destined for late endosomes. J. Cell Biol. *133*, 29–41.

Clague, M.J., Urbé, S., Aniento, F., and Gruenberg, J. (1994). Vacuolar ATPase activity is required for endosomal carrier vesicle formation. J. Biol. Chem. *269*, 21–24.

Demaurex, N., Furuya, W., D'Souza, S., Bonifacino, J.S., and Grinstein, S. (1998). Mechanism of acidification of the trans-Golgi network (TGN). In situ measurements of pH using retrieval of TGN38 and furin from the cell surface. J. Biol. Chem. *273*, 2044–2051.

Felbor, U., Kessler, B., Mothes, W., Goebel, H.H., Ploegh, H.L., Bronson, R.T., and Olsen, B.R. (2002). Neuronal loss and brain atrophy in mice lacking cathepsins B and L. Proc. Natl. Acad. Sci. USA *99*, 7883–7888.

Feliciangeli, S., Tardy, M.P., Sandoz, G., Chatelain, F.C., Warth, R., Barhanin, J., Bendahhou, S., and Lesage, F. (2010). Potassium channel silencing by constitutive endocytosis and intracellular sequestration. J. Biol. Chem. *285*, 4798–4805.

Franke, B., Neale, B.M., and Faraone, S.V. (2009). Genome-wide association studies in ADHD. Hum. Genet. *126*, 13–50.

Garbern, J.Y., Neumann, M., Trojanowski, J.Q., Lee, V.M., Feldman, G., Norris, J.W., Friez, M.J., Schwartz, C.E., Stevenson, R., and Sima, A.A. (2010). A mutation affecting the sodium/proton exchanger, SLC9A6, causes mental retardation with tau deposition. Brain *133*, 1391–1402.

Gilfillan, G.D., Selmer, K.K., Roxrud, I., Smith, R., Kyllerman, M., Eiklid, K., Kroken, M., Mattingsdal, M., Egeland, T., Stenmark, H., et al. (2008). SLC9A6 mutations cause X-linked mental retardation, microcephaly, epilepsy, and ataxia, a phenotype mimicking Angelman syndrome. Am. J. Hum. Genet. *82*, 1003–1010.

Gu, F., and Gruenberg, J. (2000). ARF1 regulates pH-dependent COP functions in the early endocytic pathway. J. Biol. Chem. *275*, 8154–8160.

Günther, W., Piwon, N., and Jentsch, T.J. (2003). The ClC-5 chloride channel knock-out mouse - an animal model for Dent's disease. Pflugers Arch. *445*, 456–462.

Hurtado-Lorenzo, A., Skinner, M., El Annan, J., Futai, M., Sun-Wada, G.H., Bourgoin, S., Casanova, J., Wildeman, A., Bechoua, S., Ausiello, D.A., et al. (2006). V-ATPase interacts with ARNO and Arf6 in early endosomes and regulates the protein degradative pathway. Nat. Cell Biol. *8*, 124–136.

Jentsch, T.J. (2007). Chloride and the endosomal-lysosomal pathway: emerging roles of CLC chloride transporters. J. Physiol. *578*, 633–640.

Kasper, D., Planells-Cases, R., Fuhrmann, J.C., Scheel, O., Zeitz, O., Ruether, K., Schmitt, A., Poët, M., Steinfeld, R., Schweizer, M., et al. (2005). Loss of the chloride channel ClC-7 leads to lysosomal storage disease and neurodegeneration. EMBO J. *24*, 1079–1091.

Kornak, U., Schulz, A., Friedrich, W., Uhlhaas, S., Kremens, B., Voit, T., Hasan, C., Bode, U., Jentsch, T.J., and Kubisch, C. (2000). Mutations in the a3 subunit of the vacuolar $H^{(+)}$-ATPase cause infantile malignant osteopetrosis. Hum. Mol. Genet. *9*, 2059–2063.

Lacroix, L., Poët, M., Maehrel, C., and Counillon, L. (2004). A mechanism for the activation of the Na/H exchanger NHE1 by intracellular acidifications and mitogens. EMBO Rep. *5*, 91–96.

Lasky-Su, J., Anney, R.J., Neale, B.M., Franke, B., Zhou, K., Maller, J.B., Vasquez, A.A., Chen, W., Asherson, P., Buitelaar, J., et al. (2008). Genome-wide association scan of the time to onset of attention deficit hyperactivity disorder. Am. J. Med. Genet. B. Neuropsychiatr. Genet. *147B*, 1355–1358.

Lee, J.H., Adler, C., Norris, M., Chu, W.J., Fugate, E.M., Strakowski, S.M., and Komoroski, R.A. (2012). 4-T 7Li 3D MR spectroscopy imaging in the brains of bipolar disorder subjects. Magn. Reson. Med. *68*, 363–368.

Lin, P.J., Williams, W.P., Luu, Y., Molday, R.S., Orlowski, J., and Numata, M. (2005). Secretory carrier membrane proteins interact and regulate trafficking of the organellar $(Na^+,K^+)/H^+$ exchanger NHE7. J. Cell Sci. *118*, 1885–1897.

Llopis, J., McCaffery, J.M., Miyawaki, A., Farquhar, M.G., and Tsien, R.Y. (1998). Measurement of cytosolic, mitochondrial, and Golgi pH in single living cells with green fluorescent proteins. Proc. Natl. Acad. Sci. USA *95*, 6803–6808.

Maranda, B., Brown, D., Bourgoin, S., Casanova, J.E., Vinay, P., Ausiello, D.A., and Marshansky, V. (2001). Intra-endosomal pH-sensitive recruitment of the Arf-nucleotide exchange factor ARNO and Arf6 from cytoplasm to proximal tubule endosomes. J. Biol. Chem. *276*, 18540–18550.

Marshansky, V., and Futai, M. (2008). The V-type H^+-ATPase in vesicular trafficking: targeting, regulation and function. Curr. Opin. Cell Biol. *20*, 415–426.

Meda, S.A., Narayanan, B., Liu, J., Perrone-Bizzozero, N.I., Stevens, M.C., Calhoun, V.D., Glahn, D.C., Shen, L., Risacher, S.L., Saykin, A.J., and Pearlson, G.D. (2012). A large scale multivariate parallel ICA method reveals novel imaging-genetic relationships for Alzheimer's disease in the ADNI cohort. Neuroimage *60*, 1608–1621.

Mellman, I. (1992). The importance of being acid: the role of acidification in intracellular membrane traffic. J. Exp. Biol. *172*, 39–45.

Mignot, C., Héron, D., Bursztyn, J., Momtchilova, M., Mayer, M., Whalen, S., Legall, A., Billette de Villemeur, T., and Burglen, L. (2013). Novel mutation in SLC9A6 gene in a patient with Christianson syndrome and retinitis pigmentosum. Brain Dev. *35*, 172–176.

Milosavljevic, N., Duranton, C., Djerbi, N., Puech, P.H., Gounon, P., Lagadic-Gossmann, D., Dimanche-Boitrel, M.T., Rauch, C., Tauc, M., Counillon, L., and Poët, M. (2010). Nongenomic effects of cisplatin: acute inhibition of mechanosensitive transporters and channels without actin remodeling. Cancer Res. *70*, 7514–7522.

Morrow, E.M., Yoo, S.Y., Flavell, S.W., Kim, T.K., Lin, Y., Hill, R.S., Mukaddes, N.M., Balkhy, S., Gascon, G., Hashmi, A., et al. (2008). Identifying autism loci and genes by tracing recent shared ancestry. Science *321*, 218–223.

Nakamura, N., Tanaka, S., Teko, Y., Mitsui, K., and Kanazawa, H. (2005). Four Na^+/H^+ exchanger isoforms are distributed to Golgi and post-Golgi

compartments and are involved in organelle pH regulation. J. Biol. Chem. *280*, 1561–1572.

Numata, M., and Orlowski, J. (2001). Molecular cloning and characterization of a novel (Na^+,K^+)/H^+ exchanger localized to the trans-Golgi network. J. Biol. Chem. *276*, 17387–17394.

Poët, M., Kornak, U., Schweizer, M., Zdebik, A.A., Scheel, O., Hoelter, S., Wurst, W., Schmitt, A., Fuhrmann, J.C., Planells-Cases, R., et al. (2006). Lysosomal storage disease upon disruption of the neuronal chloride transport protein ClC-6. Proc. Natl. Acad. Sci. USA *103*, 13854–13859.

Pouysségur, J., Sardet, C., Franchi, A., L'Allemain, G., and Paris, S. (1984). A specific mutation abolishing Na^+/H^+ antiport activity in hamster fibroblasts precludes growth at neutral and acidic pH. Proc. Natl. Acad. Sci. USA *81*, 4833–4837.

Schneider, C.A., Rasband, W.S., and Eliceiri, K.W. (2012). NIH Image to ImageJ: 25 years of image analysis. Nat. Methods *9*, 671–675.

Scott, C.C., and Gruenberg, J. (2011). Ion flux and the function of endosomes and lysosomes: pH is just the start: the flux of ions across endosomal membranes influences endosome function not only through regulation of the luminal pH. Bioessays *33*, 103–110.

Strømme, P., Dobrenis, K., Sillitoe, R.V., Gulinello, M., Ali, N.F., Davidson, C., Micsenyi, M.C., Stephney, G., Ellevog, L., Klungland, A., and Walkley, S.U. (2011). X-linked Angelman-like syndrome caused by Slc9a6 knockout in mice exhibits evidence of endosomal-lysosomal dysfunction. Brain *134*, 3369–3383.

Teter, K., Chandy, G., Quiñones, B., Pereyra, K., Machen, T., and Moore, H.P. (1998). Cellubrevin-targeted fluorescence uncovers heterogeneity in the recycling endosomes. J. Biol. Chem. *273*, 19625–19633.

Vermeulen, M., Giordano, M., Trevani, A.S., Sedlik, C., Gamberale, R., Fernández-Calotti, P., Salamone, G., Raiden, S., Sanjurjo, J., and Geffner, J.R. (2004). Acidosis improves uptake of antigens and MHC class I-restricted presentation by dendritic cells. J. Immunol. *172*, 3196–3204.

Zhang, L., Wang, T., Wright, A.F., Suri, M., Schwartz, C.E., Stevenson, R.E., and Valle, D. (2006). A microdeletion in Xp11.3 accounts for co-segregation of retinitis pigmentosa and mental retardation in a large kindred. Am. J. Med. Genet. A. *140*, 349–357.